

# **First Principles Study of Si/Ge Core-Shell nanowires under external uniaxial strain**

**Xihong Peng,<sup>1\*</sup> Fu Tang,<sup>2</sup> Paul Logan<sup>2</sup>**

<sup>1</sup>Department of Applied Sciences and Mathematics, Arizona State University, Mesa, AZ 85212

<sup>2</sup>Department of Physics, Arizona State University, Tempe, AZ 85287

## **ABSTRACT**

Density-functional theory based first principles calculations are performed to study the effects of external uniaxial strain on the electronic states of Si/Ge core-shell nanowires along the [110] direction with the diameter of the wire up to 5 nm. As shown in the calculations, the [110] Si/Ge core-shell nanowires without external strain possess a direct band gap, in contrast to the nature of an indirect band gap in bulk Si and Ge. The band structure of the core-shell nanowires can be significantly modulated by an external strain. With a sufficient amount of tensile uniaxial strain, the band gap of the Si/Ge core-shell nanowires experiences a transition from direct to indirect. In addition, our studies showed that the effective masses of charge carriers can be also tuned by the external uniaxial strain. The effective mass of the hole increases dramatically with a tensile strain, while strain shows a minimal effect on tuning the effective mass of the electron. Finally, the relationship between the strain effect and the edge states of conduction and valence bands is discussed in detail. Our results suggested strain can be used to tune the electronic properties of nanowires, which may help in design of future nano-electronic devices.

**Keywords:** Si/Ge core-shell nanowires, strain, band gap, band structure, effective mass

\* Corresponding author. E-mail: [xihong.peng@asu.edu](mailto:xihong.peng@asu.edu).

## 1. Introduction

One-dimensional semiconductor nanostructures, such as Si and Ge nanowires, have attracted extensive research efforts over the past decade [1-12]. They are expected to play important roles as both interconnects and functional components in future nanoscale electronic and optical devices, such as light-emitting diodes (LEDs) [2, 3], ballistic field-effect transistors (FETs) [5, 6], inverters [3], and nanoscale sensors [4, 9]. Experimental and theoretical investigations showed that in these nanoscale wires the charge carriers are confined in the lateral direction of the wires, thus quantum confinement effect is expected to play an important role on the electronic properties. This confinement effect has been observed, for example, in photoluminescence (PL) studies, by exhibiting substantial blue-shift of emission with reduction of the nanowire diameter [13-15]. Researchers also found that the band gap of Si and Ge nanowires depends on several factors, such as size [14-16], crystalline orientation [15-17], surface chemistry [17, 18], and doping [17, 19].

Recently, particular attention has been given to the Si/Ge core-shell nanowires, in which factors, such as heterostructure composition and interface geometry, can be further manipulated to tune the electronic properties of nanowires [18, 20-31]. Compared to pure Si and Ge wires, the core-shell structure has some superior properties. For instance, a better conductance and higher mobility of charge carries can be obtained, due to the band offsets in the core-shell nanowires [18, 23, 30]. In addition to experimental studies [27, 31], several theoretical calculations were performed to study the quantum confinement effect in Si/Ge core-shell nanowires [25, 28-30]. In these calculations, the band gap and near-gap electronic states are particularly investigated as a function of hetero-composition. For example, Wang's group [28, 29] reported the band gap of Si/Ge core-shell nanowires as a function of composition for wires with diameter up to 3 nm;

Migas *et al.* [32] studied the electronic properties of Si/Ge core-shell nanowire along the [100] direction with a diameter of 1.5 nm; Yang *et al.* [30] investigated the near-gap electronic states with the core and shell regions along [110] and [111] directions with diameter up to 4 nm.

Strain is another factor that has been demonstrated to critically affect the electronic properties of various nanostructures. Despite a few limited experimental studies of strain [23, 24], a detailed theoretical investigation of the strain effects on the electronic properties in Si/Ge core-shell nanowires is still lacking. In the Si/Ge core-shell nanowires, there will be an intrinsic strain in the nanowires, due to the lattice mismatch between Si and Ge. Recently, Peng *et al.* [33] have shown that the band gap of the core/shell nanowires can be significantly modulated by this intrinsic strain. Here we give a thorough study of the effect of the external uniaxial strain on the band structure of Si/Ge core-shell wires with diameter up to 5 nm, using first principles calculations.

## 2. Simulation details

The first principles density-functional theory (DFT) [34] calculations were performed using the Vienna computational code VASP [35, 36]. The DFT local density approximation (LDA) was applied. In detail, we used a pseudo-potential plane wave approach with kinetic energy cutoff of 200.0 eV with the key tag `PREC = Accurate`. The core electrons are described using ultra-soft Vanderbilt pseudo-potentials [37]. The reciprocal space is sampled at  $1 \times 1 \times 4$  using Monkhorst Pack meshes. We include 21 K-points in the band structure calculation along the reciprocal direction  $\Gamma$  to X. The dangling bonds on the wire surface are saturated by hydrogen atoms with initial bond lengths 1.47 Å (Si-H), and 1.51 Å (Ge-H), respectively. For Si-core/Ge-shell nanowires, the core is consisted of 30 Si atoms, and the thickness of the Ge shell is varied

(See Figure 1). Similarly, for Ge-core/Si-shell wires, the core contains 30 Ge atoms and the size of the Si shell varies. The initial lattice constant along [110] direction in the Si-core/Ge-shell nanowires is set to be 0.3977 nm, taken from the lattice constant of bulk Ge 0.5625 nm (*i.e.*  $a_{initial[110]} = a_{bulk} / \sqrt{2}$ ). The lattice along the axial direction in the Ge-core/Si-shell nanowires is initially set to be 0.3862 nm, derived from the lattice constant of bulk Si 0.5461 nm. The reason to choose such different initial lattice constant is the following. Take an example of Si-core/Ge-shell nanowires, the core consists of 30 Si atoms, while the thickness of the Ge shell is varied. Therefore, the larger the diameter of the wire, the more Ge atoms are included in the wire. The optimized lattice constant is thus expected to be more close to that of bulk Ge. Besides the axial lattice constant, the lateral size of the simulation supercell is chosen so that the distance between the wire and its replica (due to periodic boundary conditions) is more than 1.0 nm. Under this configuration, the interactions between the wire and its replica are negligible. The [110] axial lattice constant of all the core/shell wires is then optimized through the technique of total energy minimization till the force acting on atoms is less than 0.02 eV/Å. The electronic properties of the wire, such as the band structure and the gap, are then calculated by solving the Kohn-Sham equation within the frame of DFT. The band gap of a wire is defined by the energy difference between the bottom of the conduction band (conduction band edge – CBE) and the top of the valence band (valance band edge – VBE). The effective masses of the electron and the hole can be readily calculated according to the formula  $m^* = \hbar^2 / (d^2 E / dk^2)$  from the band structure of the wire.

Table 1 lists the Si/Ge core-shell wires studied in the present work. D is the diameter of a wire in the unit of nanometers, defined as the longest distance between two Ge atoms (for a Si-core/Ge-shell wire) or two Si atoms (for a Ge-core/Si-shell wire) in the cross-section of the wire;

$N_{\text{core}}/N_{\text{shell}}$  are the numbers of core/shell atoms in a given wire;  $N_{\text{H}}$  represents the number of H atoms needed to passivate the surface dangling bonds. Figure 1 gives the snapshots of three core/shell nanowires at the diameters of 2.5 nm, 3.7 nm, and 4.7 nm, viewed from the cross-section. The core and shell atoms could be either Si or Ge. The diameter of the core and the entire nanowire is also given at the bottom in the figure.

Once the geometrically optimized wire is obtained, we applied uniaxial tensile/compressive strain to the wire by scaling the axial lattice constant of the wire. The positive values of strain refer to uniaxial expansion, while negative corresponds to compression. For each strained wire, the lateral  $x$  and  $y$  coordinates are further relaxed through energy minimization. Our study showed that the band structure of the wire is affected significantly by strain.

### 3. Results and discussion

As detailed discussion of the geometrical structures of the optimized Si/Ge core-shell nanowires were described in the reference [33], here we briefly report the optimized lattice constants along the [110] direction for the studied nanowires in Table 2. In the Si-core/Ge-shell wires, the [110] axial lattice constant is increasing with the diameter of the wire, from 0.3917 nm for the 2.5 nm wire to 0.3944 nm for the 4.7 nm wire. In addition, the lattice constants for the Si-core/Ge-shell wires are smaller than  $a_{\text{initial}} = 0.3977$  nm (from bulk Ge), but larger than 0.3862 nm (from bulk Si). These results are expected since a larger Si-core/Ge-shell wire has more Ge atoms. On the other hand, the lattice constant of the Ge-core/Si-shell wires is reduced with size, from 0.3985 nm to 0.3900 nm. With these optimized axial lattice constants, an intrinsic strain has been produced in the Si/Ge core-shell nanowires. The Si composition is in an intrinsic tensile strain, while the Ge composition experiences an intrinsic compressive strain [33].

## I. Electron charge distribution of conduction and valence bands

Figure 2 shows the isovalue surfaces of the charge density of the valence/conduction band edges in the nanowires with the diameters 2.5 nm and 3.7 nm. From the figures viewed in the cross sections (i.e. in the  $xy$  plane), we can see that the charge of VBE in the Si-core/Ge-shell wires is mainly distributed in the Ge shell, while the charge of CBE is mainly located in the Si core, as shown in Figure 2(a) and 2(b). On the other hand, the charge of VBE in the Ge-core/Si-shell wires is primarily in the Ge core, while the charge of CBE is distributed in the Si shell, shown in Figure 2(c) and 2(d). In conclusion, the VBE charge is in the Ge composition while the CBE charge is in the Si composition, regardless of whether the nanowire is of a Si-core/Ge-shell or Ge-core/Si-shell structure [30]. As discussed in the reference [33], with the intrinsic strain in the core/shell structures, the confined distribution of the electron charge results in a reduced band gap compared with that of pure Si or Ge nanowires.

## II. Band gaps

Bulk Si and Ge are indirect band gap materials. However, the Si/Ge core-shell and the pure Si and Ge nanowires along the  $[110]$  direction demonstrate a direct band gap at  $\Gamma$  [14, 16, 17]. As mentioned before, the band gap of a Si/Ge core-shell wire is defined by the energy difference between CBE and VBE. The DFT predicted band gaps for the Si/Ge core-shell wires are given in Table 2. The gap is increased with reducing wire size, which is mainly due to the quantum confinement effect. It is known that DFT underestimates band gaps of semiconductors, while advanced GW method [38-40] and quantum Monte Carlo calculations [41-43] provide improved predictions. However, previous studies [44] on Si nanoclusters and nanowires showed that the

DFT gap predicts a similar size-dependency as the optical gap obtained using GW and quantum Monte Carlo methods [41, 43].

Our calculations show that the band structure and the band gap of the Si/Ge core-shell nanowires are notably modulated with strain. The variation of the band gap as a function of uniaxial strain for both the Si-core/Ge-shell and the Ge-core/Si-shell nanowires are plotted in Figure 3. It is clear that strain can modify the band gap. Generally, the gap is decreased evidently under expansion, while it only slightly varies with compression. More interestingly, under a sufficient extension, the nanowires with a larger diameter have a transition from a direct gap to an indirect gap, which are indicated by green arrows in Figure 3. This transition will be discussed in detail in next section.

In order to explain the general trend presented in Figure 3, i.e. the gap reducing with the uniaxial tensile strain, we further examined the energies of CBE and VBE. As an example, in Figure 4, we present the energy variations of CBE and VBE with strain in the Si-core/Ge-shell nanowire with a diameter of 2.5 nm. Note that the similar behavior is also observed for other wires. From Figure 4, the energies of CBE and VBE are both decreased with the tensile strain and the CBE curve has a lightly larger slope compared to that of the VBE curve (thus giving a reduced gap under the tensile strain). The physical origin of the curves may be understandable from the wave-functions of CBE and VBE. In Table 3, we listed the projections of the wave-functions of various electron states on  $s$ ,  $p$ ,  $d$  states onto spherical harmonics centered at the positions of the Si/Ge atoms with a radius of 1.2 Å. From the table, we can see that for the Si-core/Ge-shell nanowire, the VBE state (i. e. valence band at  $\Gamma$ ) is dominated by  $p_z$  character. This  $p_z$  orbit suggests that the nodal surfaces of the positive and negative values of the wave-function will be perpendicular to the wire axis [45, 46]. When the nanowire is under tensile strain, the

distance between nodal surfaces will increase. In this case, the kinetic energy associated with the transportation of the electron between atoms reduces [46]. So does the VBE energy. For the CBE energy, the projected wave-function includes a significant  $d_{z^2}$  character. As demonstrated by other researchers [47-49], the  $d$  character defines the crystalline electronic state of the conduction band. Similar to the  $p_z$  character, the  $d_{z^2}$  orbit also produces nodal surfaces perpendicular to the wire axis. Therefore, the CBE energy becomes smaller as the nanowire is under extension.

From the charge distribution of CBE and VBE shown in Figure 2(a), we can see that the charge of VBE and CBE are mainly located in the Ge-shell and Si-core, respectively. The confined distributions of the electron charge give a clue to why the CBE curve in Figure 4 has a larger slope compared to that of VBE curve. For the relaxed 2.5 nm Si-core/Ge-shell nanowire (i.e. no external strain has been applied), the intrinsic strain in the Si-core and the Ge-shell are +1.5% and -1.5%, respectively, due to the lattice mismatch of Si and Ge [33]. If a +2% external tensile strain is applied to the wire, the resulting strain in the Si-core and Ge-shell are approximately 3.5% and 0.5%, compared to bulk. Thus we expect the Si atoms in the core are more effectively expanded compared to those of the Ge atoms in the shell. Since the charge of CBE is mainly located in the Si-core while the electron of VBE is in the Ge-shell, the energy of CBE will have a larger reduction compared to that of VBE under expansion.

### III. Energy dispersive curves and effective masses

The effective masses of the electron and the hole can be obtained from the band structure of the nanowires according to  $m^* = \hbar^2 / (d^2 E / dk^2)$ . In Table 2, we report the calculated effective masses.  $m_e^*$  represents the effective mass of the electron, while  $m_h^*$  is the effective mass of the hole, in unit of the free electron mass  $m_e$ . For example, the effective mass of the electron  $m_e^*$  in



the core/shell wires are  $0.13 m_e$  or  $0.14 m_e$ , having a negligible change with size. On the other hand, the effective mass of the hole is dependent on the wire size. The wire with a diameter of 3.7 nm has the largest effective mass of the hole, for both Si-core and Ge-core wires.

We further studied the effect of the external strain on the effective masses of the electron and the hole. For example, in order to calculate the effective masses for the Ge-core/Si-shell wire with a diameter of 2.5 nm, the dispersion relation with the wave vector  $K$  in the range of  $\pm 0.2 \cdot \frac{2\pi}{a}$  in the region near  $\Gamma$  is plotted under different values of strain, as shown in Figure 5(a).

Strain shows a dominant effect on the band structure at  $\Gamma$  - the energies are shifted evidently with strain. However, the strain has negligible effects on the bands for wave vectors far away from  $\Gamma$

( $K > 0.15 \cdot \frac{2\pi}{a}$  or  $K < -0.15 \cdot \frac{2\pi}{a}$ ) - a minimal energy shift under strain [33]. The K-point-

dependence strain effect can be understood from the tight-binding model [50]. Here, we directly investigated the wave-functions of the valence/conduction bands at two different wave vectors,

namely  $\Gamma$  and  $K = 0.20 \cdot \frac{2\pi}{a}$ , as shown in Table 3. For the valence/conduction band at  $\Gamma$ , the

significant portion of  $p_z/d_{z^2}$  character exist. Therefore the energy of the valence/conduction band at  $\Gamma$  will shift down with an external tensile strain (see the above section of Figure 4). However,

for the wave-functions at  $K = 0.20 \cdot \frac{2\pi}{a}$ , the portions of these two types of character are largely

reduced, while  $p_x$  or  $p_y$  character dominates. In this case the nodal surfaces will be mainly parallel to the axis of the nanowire. The extension of the nanowire will not change the distance

between the nodal surfaces. Therefore, the kinetic energy associated with the electron

transportation stays the same. This explains the minimal band energy shift under strain at a large wave vector [46].

From Figure 5(a), the conduction band edge is located at  $\Gamma$ , regardless of the applied strain. However, the valence band edges demonstrate an interesting transition – the VBE is no longer located at  $\Gamma$  for a larger extensile strain such as +1.8%, implying an indirect band gap. An enlarged graph of the valence band near  $\Gamma$  under 1.8% extension is presented in Figure 5(b). The real valence band edge is determined by the two states labeled as  $v_0$  at  $\Gamma$  and  $v_I$  near  $K = 0.05 \cdot \frac{2\pi}{a}$ . Without strain (refer to the pink solid-square curve in Figure 5(a)),  $v_0$  is higher than  $v_I$ , the wire demonstrates a direct band gap with both CBE and VBE at  $\Gamma$ . Under 1.8% uniaxial extension, the shift-down of  $v_0$  is more significant than that of  $v_I$ , so that  $v_I$  becomes the valence band edge, resulting in an indirect band gap. This direct to indirect band gap transition also happens for the larger wires under sufficient tensile strain (see data points in Figure 2 indicated by green arrows).

At last, the effective masses of the electron and the hole under external uniaxial strain are calculated based on the energy dispersion curves and plotted in Figure 6. The variations of the effective masses of the electron with strain for the three smaller wires, 2.5 nm, 3.0 nm and 3.7 nm are minimal (see Figure 6(a) and 6(b)). And for the largest wire with the diameter of 4.7 nm, the effective mass of the electron increases slightly with compressive strain. In contrast, the change of the effective mass of the hole is dramatic, as shown in Figure 6(c) and 6(d). For example, for the Ge-core/Si-shell wire with the diameter 2.5 nm – the diamond curve in Figure 6(d), the effective mass of the hole decreases from  $0.21 m_e$  without strain to  $0.15 m_e$  under 2.2% compression, resulting from the sharper curvature of the valence band dispersion relation in

Figure 5(a) (shown by the black solid-dot and pink solid-square curves). In the case of 3.0 nm Ge-core/Si-shell wire (see Figure 6(d)), the effective mass of the hole decreases slightly from  $0.166 m_e$  without strain to  $0.145 m_e$  under -2.3% compression (decreased by 13%), while the mass dramatically increases to  $0.728 m_e$  under 0.7% tensile strain (increased by 338%). When the tensile strain is beyond 0.7% for this wire, the VBE is shifted away from  $\Gamma$ , the effective mass of the hole parabolically fitted from the new VBE gets reduced to  $0.453 m_e$  under 1.7% strain. Similar behavior is also observed for other wires, as shown in Figure 6(c) and 6(d).

#### 4. Conclusion

In summary, we found that (1) the band structures of Si/Ge core-shell nanowires along [110] direction can be tuned by external uniaxial strain; (2) the band gap of the wire varies with strain; (3) strain affects the effective masses of the electron and the hole in a different manner: strain has a minimal effect in changing the effective mass of the electron, while it can dramatically modify the effective mass of the hole. Our studies show that the effective mass of the hole can be reduced by tuning the diameter of the wire and applying appropriate strain, which supports the motivation for using Si/Ge core-shell nanowires as components and interconnects in future nanoelectronics.

#### Acknowledgement

This work is supported by the Research Initiative Fund from Arizona State University (ASU) to Peng. We are very thankful to the following for providing computational resources: ASU Fulton High Performance Computing Initiative (Cluster Saguaro), National Center for

Supercomputing Applications and Pittsburgh Supercomputing Center. Jeff Drucker is acknowledged for helpful discussions.

#### REFERENCES:

- [1] Hu B Y-K and Das Sarma S 1992 Many-body properties of a quasi-one-dimensional semiconductor quantum wire *Phys. Rev. Lett.* **68** 1750-1753
- [2] Hirschman K D, Tsybeskov L, Duttagupta S P and Fauchet P M 1996 Silicon-based visible light-emitting devices integrated into microelectronic circuits *Nature* **384** 338-341
- [3] Cui Y and Lieber C M 2001 Functional nanoscale electronic devices assembled using silicon nanowire building blocks *Science* **291** 851-853
- [4] Cui Y, Wei Q Q, Park H K and Lieber C M 2001 Nanowire nanosensors for highly sensitive and selective detection of biological and chemical species *Science* **293** 1289-1292
- [5] Cui Y, Zhong Z H, Wang D L, Wang W U and Lieber C M 2003 High performance silicon nanowire field effect transistors *Nano Lett.* **3** 149-152
- [6] Koo S M, Fujiwara A, Han J P, Vogel E M, Richter C A and Bonevich J E 2004 High inversion current in silicon nanowire field effect transistors *Nano Lett.* **4** 2197-2201
- [7] Morales A M and Lieber C M 1998 A laser ablation method for the synthesis of crystalline semiconductor nanowires *Science* **279** 208-211
- [8] Holmes J D, Johnston K P, Doty R C and Korgel B A 2000 Control of thickness and orientation of solution-grown silicon nanowires *Science* **287** 1471-1473
- [9] Hahn J and Lieber C M 2004 Direct ultrasensitive electrical detection of DNA and DNA sequence variations using nanowire nanosensors *Nano Lett.* **4** 51-54

- [10] Audoit G, Ni Mhuirheartaigh T, Lipson S M, Morris M A, Blau W J and Holmes J D 2005 Strain induced photoluminescence from silicon and germanium nanowire arrays *J. Mater. Chem.* **15** 4809-4815
- [11] Wu X Y, Kulkarni J S, Collins G, Petkov N, Almecija D, Boland J J, Ertz D and Holmes J D 2008 Synthesis and electrical and mechanical properties of silicon and germanium nanowires *Chem. Mat.* **20** 5954-5967
- [12] Dailey E and Drucker J 2009 "Seedless" vapor-liquid-solid growth of Si and Ge nanowires: The origin of bimodal diameter distributions *J. Appl. Phys.* **105** 064317-064321
- [13] Wu Z, Neaton J B and Grossman J C 2008 Quantum confinement and electronic properties of tapered silicon nanowires *Phys. Rev. Lett.* **100** 246804-246807
- [14] Beckman S P, Han J and Chelikowsky J R 2006 Quantum confinement effects in Ge [110] nanowires *Phys. Rev. B* **74** 165314-165318
- [15] Bruno M, Palummo M, Marini A, Del Sole R, Olevano V, Kholod A N and Ossicini S 2005 Excitons in germanium nanowires: Quantum confinement, orientation, and anisotropy effects within a first-principles approach *Phys. Rev. B* **72** 153310-153313
- [16] Arantes J T and Fazzio A 2007 Theoretical investigations of Ge nanowires grown along the [110] and [111] directions *Nanotechnology* **18** 295706-295710
- [17] Medaboina D, Gade V, Patil S K R and Khare S V 2007 Effect of structure, surface passivation, and doping on the electronic properties of Ge nanowires: A first-principles study *Phys. Rev. B* **76** 205327-2053213

- [18] Kagimura R, Nunes R W and Chacham H 2007 Surface dangling-bond states and band lineups in hydrogen-terminated Si, Ge, and Ge/Si nanowires *Phys. Rev. Lett.* **98** 026801-026805
- [19] Peelaers H, Partoens B and Peeters F M 2007 Properties of B and P doped Ge nanowires *Appl. Phys. Lett.* **90** 263103-263105
- [20] Lauhon L J, Gudixsen M S, Wang C L and Lieber C M 2002 Epitaxial core-shell and core-multishell nanowire heterostructures *Nature* **420** 57-61
- [21] Wu Y Y, Fan R and Yang P D 2002 Block-by-block growth of single-crystalline Si/SiGe superlattice nanowires *Nano Lett.* **2** 83-86
- [22] Lu W, Xiang J, Timko B P, Wu Y and Lieber C M 2005 One-dimensional hole gas in germanium/silicon nanowire heterostructures *Proc. Natl. Acad. Sci. U. S. A.* **102** 10046-10051
- [23] Goldthorpe I A, Marshall A F and McIntyre P C 2008 Synthesis and strain relaxation of Ge-core/Si-shell nanowire arrays *Nano Lett.* **8** 4081-4086
- [24] Trammell T E, Zhang X, Li Y L, Chen L Q and Dickey E C 2008 Equilibrium strain-energy analysis of coherently strained core-shell nanowires *J. Cryst. Growth* **310** 3084-3092
- [25] Amato M, Palummo M and Ossicini S 2009 Reduced quantum confinement effect and electron-hole separation in SiGe nanowires *Phys. Rev. B* **79** 201302- 201305
- [26] Hu J Q, Bando Y and Golberg D 2009 Novel semiconducting nanowire heterostructures: Synthesis, properties and applications *J. Mater. Chem.* **19** 330-343
- [27] Varahramyan K M, Ferrer D, Tutuc E and Banerjee S K 2009 Band engineered epitaxial Ge-Si<sub>x</sub>Ge<sub>1-x</sub> core-shell nanowire heterostructures *Appl. Phys. Lett.* **95** 033101-033103

- [28] Musin R N and Wang X Q 2006 Quantum size effect in core-shell structured silicon-germanium nanowires *Phys. Rev. B* **74** 165308-165312
- [29] Musin R N and Wang X Q 2005 Structural and electronic properties of epitaxial core-shell nanowire heterostructures *Phys. Rev. B* **71** 155318-155321
- [30] Yang L, Musin R N, Wang X Q and Chou M Y 2008 Quantum confinement effect in Si/Ge core-shell nanowires: First-principles calculations *Phys. Rev. B* **77** 195325- 195329
- [31] Yang J E, Jin C B, Kim C J and Jo M H 2006 Band-gap modulation in single-crystalline  $\text{Si}_{1-x}\text{Ge}_x$  nanowires *Nano Lett.* **6** 2679-2684
- [32] Migas D B and Borisenko V E 2007 Structural, electronic, and optical properties of <001>-oriented SiGe nanowires *Phys. Rev. B* **76** 035440-035448
- [33] Peng X H and Logan P 2010 Electronic properties of strained Si/Ge core-shell nanowires *Appl. Phys. Lett.* **96** 143119-143121
- [34] Kohn W and Sham L J 1965 Self-consistent equations including exchange and correlation effects *Phys. Rev.* **140** 1133-1138
- [35] Kresse G and Furthmuller J 1996 Efficiency of ab-initio total energy calculations for metals and semiconductors using a plane-wave basis set *Comput. Mater. Sci.* **6** 15-50
- [36] Kresse G and Furthmuller J 1996 Efficient iterative schemes for ab initio total-energy calculations using a plane-wave basis set *Phys. Rev. B* **54** 11169-11186
- [37] Vanderbilt D 1990 Soft self-consistent pseudopotentials in a generalized eigenvalue formalism *Phys. Rev. B* **41** 7892-7895
- [38] Hedin L 1965 New method for calculating the one-particle Green's function with application to the electron-gas problem *Phys. Rev.* **139** A796-A823

- [39] Faleev S V, van Schilfgaarde M and Kotani T 2004 All-electron self-consistent GW approximation: Application to Si, MnO, and NiO *Phys. Rev. Lett.* **93** 126406-126409
- [40] Bruneval F, Sottile F, Olevano V, Del Sole R and Reining L 2005 Many-body perturbation theory using the density-functional concept: Beyond the GW approximation *Phys. Rev. Lett.* **94** 186402-186405
- [41] Puzder A, Williamson A J, Grossman J C and Galli G 2002 Surface chemistry of silicon nanoclusters *Phys. Rev. Lett.* **88** 097401-097404
- [42] Williamson A J, Grossman J C, Hood R Q, Puzder A and Galli G 2002 Quantum Monte Carlo calculations of nanostructure optical gaps: Application to silicon quantum dots *Phys. Rev. Lett.* **89** 196803-196806
- [43] Zhao X, Wei C M, Yang L and Chou M Y 2004 Quantum confinement and electronic properties of silicon nanowires *Phys. Rev. Lett.* **92** 236805-236808
- [44] Peng X H, Ganti S, Alizadeh A, Sharma P, Kumar S K and Nayak S K 2006 Strain-engineered photoluminescence of silicon nanoclusters *Phys. Rev. B* **74** 035339-035343
- [45] Leu P W, Svizhenko A and Cho K 2008 Ab initio calculations of the mechanical and electronic properties of strained Si nanowires *Phys. Rev. B* **77** 235305-235318
- [46] Wu Z G, Neaton J B and Grossman J C 2009 Charge separation via strain in silicon nanowires *Nano Lett.* **9** 2418-2422
- [47] Richard S, Aniel F, Fishman G and Cavassilas N 2003 Energy-band structure in strained silicon: A 20-band k-p and Bir-Pikus Hamiltonian model *J. Appl. Phys.* **94** 1795-1799
- [48] Ren S Y, Chen X and Dow J D 1998 Tight-binding  $sp^3d^5$  Hamiltonian for Si *J. Phys. Chem. Solids* **59** 403-410



- [49] Filonov A B, Tralle I E, Petrov G V and Borisenko V E 1995 Silicon band-structure calculations by the self-consistent crystalline orbital method *Modell. Simul. Mater. Sci. Eng* **3** 45-52
- [50] Logan P and Peng X H 2009 Strain-modulated electronic properties of Ge nanowires: A first-principles study *Phys. Rev. B* **80** 115322-115328

### Table captions

**Table 1** A list of studied Si/Ge core-shell nanowires along [110] direction in present work.  $D$  is the diameter of a wire;  $N_{\text{core}}$  and  $N_{\text{shell}}$  are the numbers of Si/Ge atoms in the core and the shell of a given wire;  $N_{\text{H}}$  is the number of H atoms needed to saturate the surface dangling bonds.

**Table 2** The optimized axial lattice constants, the DFT predicted energy gap and effective masses of the electron and the hole in Si/Ge core-shell nanowires along [110] direction.

**Table 3** Projections of the valence band (VB) and the conduction band (CB) onto the  $s$ ,  $p$ , and  $d$  states in the 2.5 nm wires.

## Figure captions

**Figure 1** Snapshots of Si/Ge core-shell nanowires with varying sizes viewed from the wire cross-section. Blue dots are shell atoms (Ge or Si), yellow are core atoms (Si or Ge), white are passivating H atoms. The diameters of the core and the whole wire are reported below.

**Figure 2** The isovalue surfaces of the charge density of the valence/conduction band edges in Si/Ge core-shell nanowires. The yellow, blue and white balls represent Si, Ge, and H atoms, respectively.

**Figure 3** The change of the DFT predicted band gap in Si/Ge core-shell wires as a function of uniaxial strain  $\varepsilon$  at different size. Positive strain refers to uniaxial expansion while negative strain corresponds to its compression. (The data points indicated by an arrow are for indirect band gaps.)

**Figure 4** The energy variation of CBE and VBE with the external strain in the Si-core/Ge-shell nanowire with the diameter of 2.5 nm. The vertical axis  $\Delta$  energy is defined as the CBE/VBE energy differences between the strained and the relaxed wire.

**Figure 5** The conduction and the valence bands of a Ge-core/Si-shell wire with a diameter of 2.5 nm at the near region of  $\Gamma$  are plotted under different values of uniaxial strain. The rectangle enclosed curve under 1.8% strain has been enlarged in (b), indicating an indirect band gap with the valence band edge located at state  $v_I$  rather than  $v_0$ .

**Figure 6** The effective masses of the electron (top) and hole (bottom) are plotted as a function of uniaxial strain for Si/Ge core-shell nanowires at different size. It shows that the effective mass of the electron changes mildly with strain. However, the effective mass of the hole reduces under compression, while enhanced dramatically with tensile strain.

D (nm)	N <sub>core</sub>	N <sub>shell</sub>	N <sub>H</sub>
2.5	30	46	28
3.0	30	80	32
3.7	30	142	44
4.7	30	246	52

**Table 1, Peng *et al.***

	Diameter (nm)	Optimized Axial Lattice (nm)	E <sub>g</sub> (eV)	m <sub>e</sub> <sup>*</sup>	m <sub>h</sub> <sup>*</sup>
Si-core /Ge-shell	2.5	0.3917	0.54	0.13	0.16
	3.0	0.3945	0.29	0.13	0.21
	3.7	0.3965	0.18	0.14	0.32
	4.7	0.3944	0.13	0.14	0.26
Ge-core /Si-shell	2.5	0.3985	0.58	0.14	0.21
	3.0	0.3950	0.31	0.13	0.17
	3.7	0.3931	0.23	0.14	0.74
	4.7	0.3900	0.18	0.14	0.36

**Table 2, Peng *et al.***

wire	state	$ s\rangle$	$ p_x\rangle$	$ p_y\rangle$	$ p_z\rangle$	$ d_{xy}\rangle$	$ d_{yz}\rangle$	$ d_{z^2}\rangle$	$ d_{xz}\rangle$	$ d_{x^2}\rangle$
2.5 nm	VB at $\Gamma$	0.014	0.000	0.000	0.995	0.000	0.099	0.000	0.002	0.000
Si-core	VB at $0.2\cdot 2\pi/a$	0.045	0.967	0.212	0.098	0.095	0.008	0.011	0.003	0.005
/Ge-shell	CB at $\Gamma$	0.596	0.022	0.585	0.000	0.000	0.000	0.547	0.000	0.044
	CB at $0.2\cdot 2\pi/a$	0.603	0.155	0.532	0.054	0.012	0.006	0.066	0.006	0.567
2.5 nm	VB at $\Gamma$	0.008	0.000	0.000	0.995	0.000	0.097	0.000	0.002	0.000
Ge-core	VB at $0.2\cdot 2\pi/a$	0.059	0.991	0.073	0.018	0.089	0.002	0.005	0.005	0.002
/Si-shell	CB at $\Gamma$	0.588	0.022	0.669	0.000	0.005	0.000	0.452	0.000	0.044
	CB at $0.2\cdot 2\pi/a$	0.646	0.152	0.545	0.108	0.038	0.025	0.063	0.013	0.494

**Table 3, Peng *et al.***

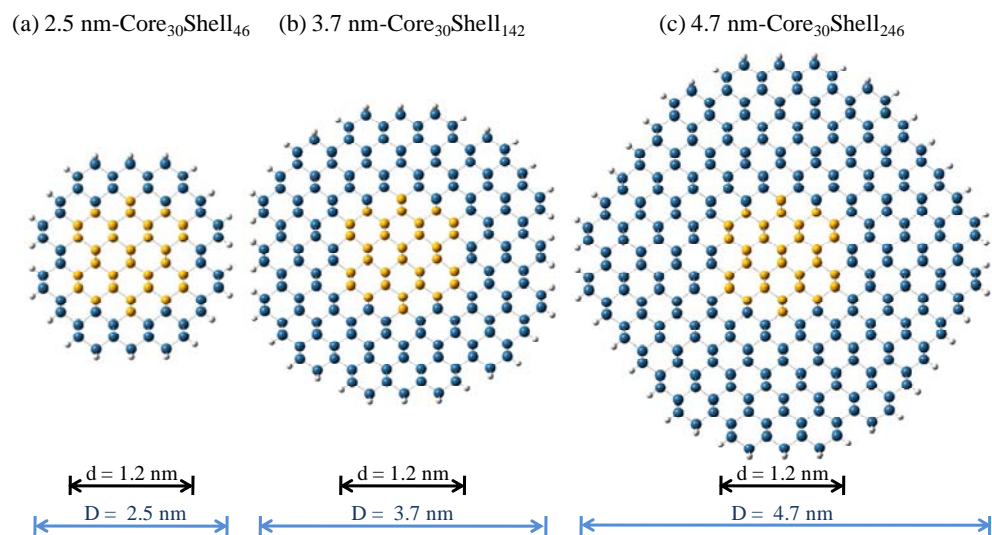


**Figure 1, Peng *et al.***

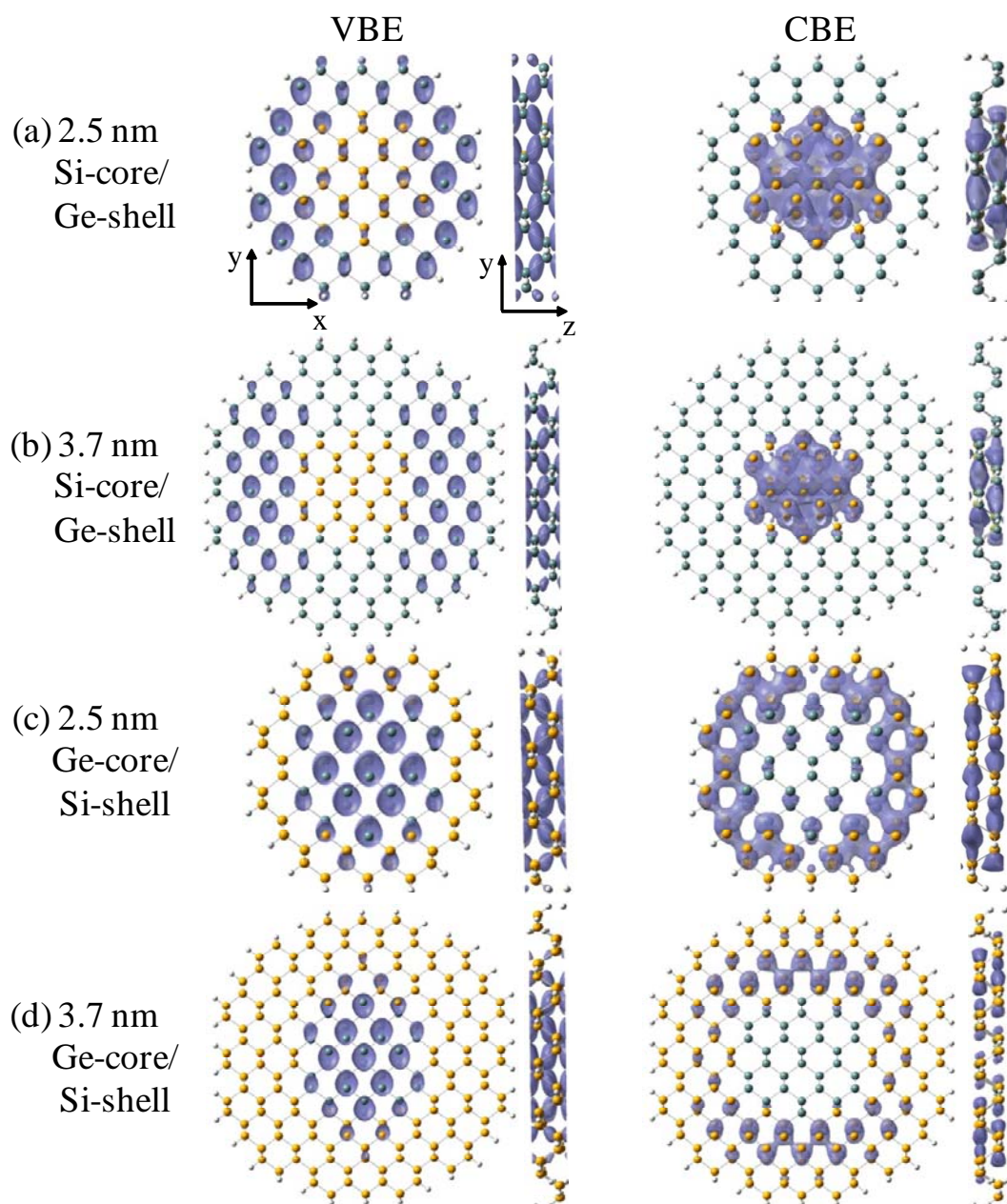


**Figure 2, Peng *et al.***

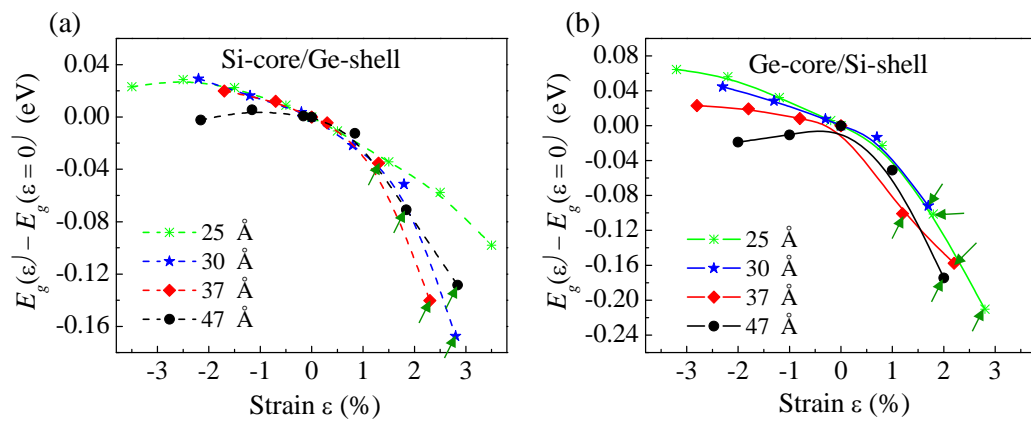


**Figure 3, Peng *et al.***

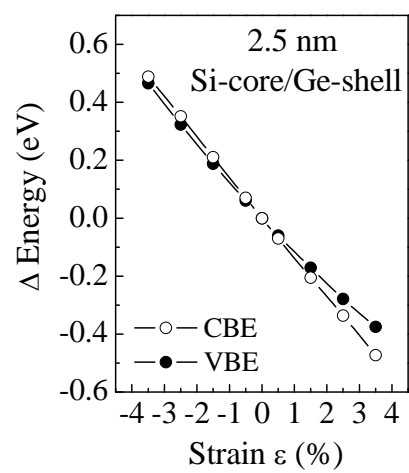


**Figure 4, Peng *et al.***



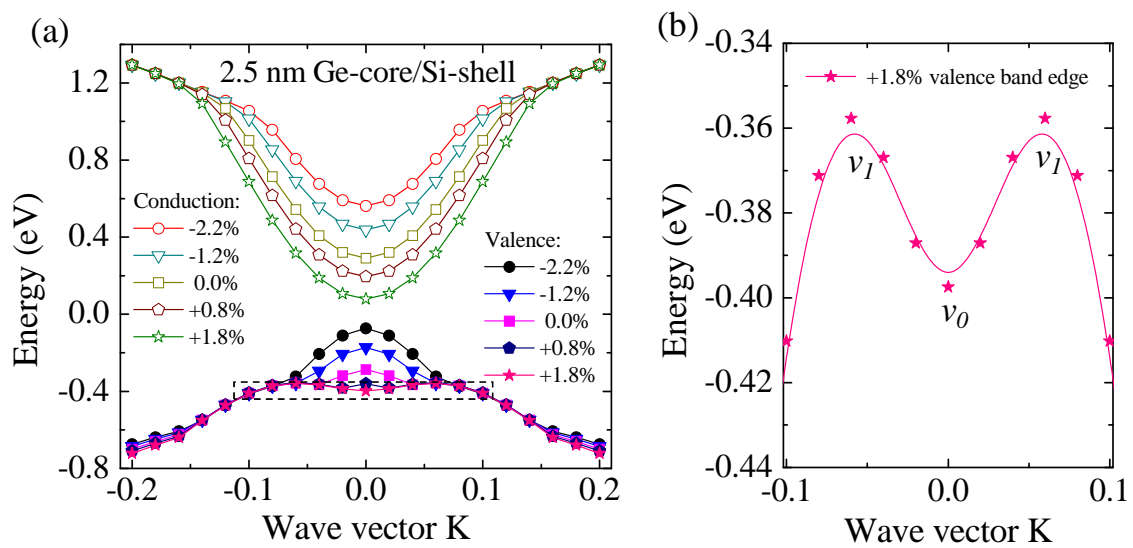


Figure 5, Peng *et al.*

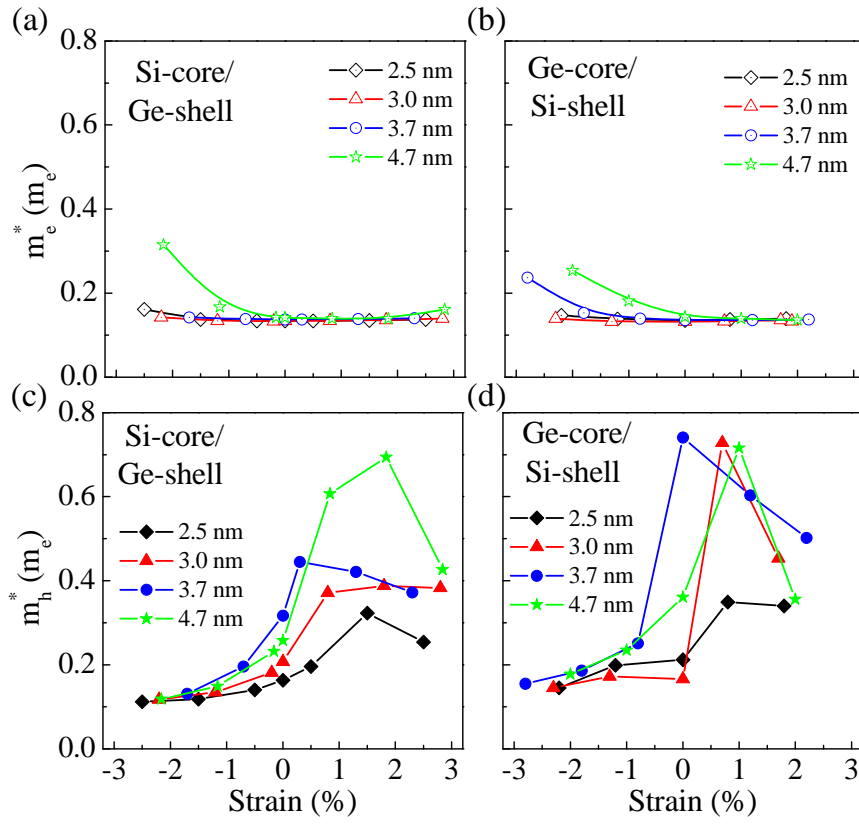


Figure 6, Peng *et al.*